



# A role for astrocytic insulin-like growth factor I receptors in the response to ischemic insult

Kentaro Suda<sup>1,2</sup>, Jaime Pignatelli<sup>1,3</sup>, Laura Genis<sup>1,3</sup>, Ana M Fernandez<sup>1,3</sup>, Estrella Fernandez de Sevilla<sup>1,3</sup> , Ines Fernandez de la Cruz<sup>1</sup>, Andrea Pozo-Rodrigalvarez<sup>1</sup>, Maria L de Ceballos<sup>1</sup>, Sonia Díaz-Pacheco<sup>1</sup>, Raquel Herrero-Labrador<sup>1,3</sup> and Ignacio Torres Aleman<sup>3,4,5</sup> 

## Abstract

Increased neurotrophic support, including insulin-like growth factor I (IGF-I), is an important aspect of the adaptive response to ischemic insult. However, recent findings indicate that the IGF-I receptor (IGF-IR) in neurons plays a detrimental role in the response to stroke. Thus, we investigated the role of astrocytic IGF-IR on ischemic insults using tamoxifen-regulated Cre deletion of IGF-IR in glial fibrillary acidic protein (GFAP) astrocytes, a major cellular component in the response to injury. Ablation of IGF-IR in astrocytes (GFAP-IGF-IR KO mice) resulted in larger ischemic lesions, greater blood-brain-barrier disruption and more deteriorated sensorimotor coordination. RNAseq detected increases in inflammatory, cell adhesion and angiogenic pathways, while the expression of various classical biomarkers of response to ischemic lesion were significantly increased at the lesion site compared to control littermates. While serum IGF-I levels after injury were decreased in both control and GFAP-IR KO mice, brain IGF-I mRNA expression show larger increases in the latter. Further, greater damage was also accompanied by altered glial reactivity as reflected by changes in the morphology of GFAP astrocytes, and relative abundance of ionized calcium binding adaptor molecule 1 (Iba 1) microglia. These results suggest a protective role for astrocytic IGF-IR in the response to ischemic injury.

## Keywords

Insulin-like growth factor, astrocytes, stroke, neuroprotection, Cre deletion

Received 20 March 2023; Revised 17 October 2023; Accepted 27 October 2023

## Introduction

Brain stroke is the second cause of death worldwide,<sup>1</sup> and current life-style, that increases its risks factors, dims hope for improvement.<sup>2</sup> Albeit new therapeutic options are promising,<sup>3,4</sup> this condition is still a significant clinical burden demanding fresh insights if we want to reach better therapeutic outcomes.<sup>5</sup> Endogenous neuroprotective pathways involving a myriad of homeostatic processes, that are highest during the subacute phase of response to ischemic damage,<sup>5</sup> help restore function up to a certain degree after injury in many patients.<sup>6</sup> Undoubtedly, a better knowledge of the processes involved in spontaneous recovery may lead to new therapeutic approaches by mimicking or potentiating them.

<sup>1</sup>Cajal Institute, Consejo Superior de Investigaciones Científicas, Madrid, Spain

<sup>2</sup>Division of Diabetes and Endocrinology, Department of Internal Medicine, Kobe University Graduate School of Medicine, Kobe, Japan

<sup>3</sup>CIBERNED, Madrid, Spain

<sup>4</sup>Achucarro Basque Center for Neuroscience, Leioa, Spain

<sup>5</sup>Ikerbasque Basque Foundation for Science, Bilbao, Spain

### Corresponding authors:

Kentaro Suda, Division of Diabetes and Endocrinology, Department of Internal Medicine, Kobe University Graduate School of Medicine, 7-5-1 Kusunoki-cho, Chuo-ku, Kobe City, Hyogo, Japan.  
Email: suda.kn.aqua@gmail.com

Ignacio Torres Aleman, Achucarro Basque Center for Neuroscience, Barrio Sarriena, s/n E-48940 Leioa (Bizkaia), Spain.  
Email: ignacio.torres@achucarro.org

Insulin-like growth factor I (IGF-I) is considered a prototypical neurotrophic factor participating in protection against oxidative stress and inflammation,<sup>7,8</sup> two pathological cascades involved in stroke pathology.<sup>9</sup> IGF-I has been reported beneficial in clinical studies of different brain illnesses,<sup>10–13</sup> and has been directly linked to stroke outcome.<sup>14,15</sup> In this regard, different reports have shown that treatment of brain stroke with IGF-I is beneficial.<sup>16–18</sup> Accordingly, IGF-I receptors (IGF-IR) are involved in IGF-I neuroprotection,<sup>19</sup> including brain ischemia in infant mice.<sup>20</sup> However, reduced levels of serum IGF-I<sup>21</sup> and serum GH/IGF-I,<sup>22</sup> or inactivation of the neuronal IGF-IR,<sup>23</sup> was shown to be also protective against ischemic injury in adult mice. Since timing is a key determinant in stroke protection,<sup>5</sup> and these studies included experimental manipulation prior to insult, the role of this neuroprotective pathway in the response to ischemia needs further clarification.

In the present study we have re-examined the role of IGF-IR in stroke injury following the same timing; i.e.: manipulating it prior to insult. We have found that in opposition to what was seen in mice with impaired IGF-IR activity in neurons,<sup>23</sup> reducing IGF-IR activity in astrocytes resulted in increased damage after ischemic injury. Greater functional impairment and larger glial reactivity were linked with greater damage.

Based on these observations we suggest that the astrocytic IGF-IR is involved in neuroprotective responses to brain damage after ischemia and that this protection overcomes the apparent deleterious role of neuronal IGF-IR in the response to stroke. These results provide a more nuanced role of IGF-I signaling in brain ischemia, emphasizing cell- and context-dependent actions of this neurotrophic factor that need to be accounted for when designing potential new treatments.

## Methods

### Animals

Animals were kept under light/dark, (12 h/12h) conditions following EU guidelines (directive 86/609/EEC) and handled according to institutionally-approved procedures (Government of the Comunidad de Madrid, Proex 112/16). Animals were fed *ad libitum* with laboratory rodent chow and kept in standard laboratory cage conditions (4 mice/cage). All efforts were made to minimize suffering and to reduce the number of animals. Procedures were according to ARRIVE 2.0 guidelines on how to report animal experiments.

Transgenic mice with tamoxifen-regulated deletion of IGF-IR in astrocytes (GFAP-IGF-IR KO mice) were obtained by crossing IGF-IR<sup>f/f</sup> mice of B6, 129

background (IGF-IR<sup>f/f</sup> mice; Jackson Labs; stock number: 012251) with CreERT2.GFAP mice of C57BL/6xSJL/J background (Jackson Labs, stock number: 012849, see<sup>24</sup> for further details). Mice lacking insulin receptors (IR) in astrocytes were obtained as described,<sup>25</sup> by crossing IR<sup>f/f</sup> mice (B6.129S4(FVB)-Insr<sup>tm1Khn</sup>/JRRID:IMSR, Jackson labs; stock number 006955) with CreERT2.GFAP mice. Tamoxifen was injected for 5 consecutive days intraperitoneally (75 mg/kg, Sigma) at the age of 2 month, and animals were used a month later. GFAP-IGF-IR mice were treated with vehicle (corn oil). Using the tdTomato/eGFP reporter mouse to detect Cre-mediated deletion in response to tamoxifen administration in CreERT2.GFAP mice, we previously documented that it was restricted to astrocytes.<sup>25</sup> Multiplex PCR for mouse genotyping included a common forward primer (P3, 5'–CTG TTT ACC ATG GCT GAG ATC TC–3') and two reverse primers specific for the wild-type (P4, 5'–CCA AGG ATA TAA CAG ACA CCA TT–3') and mutant (P2, 5'–CGC CTC CCC TAC CCG GTA GAA TTC–3') alleles. GFAP-IGF-IR KO mice show reduced brain IGF-IR levels (Suppl Figure 1A), normal levels of serum IGF-I (Suppl Fig 1B) and normal brain size. This differs from mice lacking IGF-IR in neurons, that show high serum IGF-I levels.<sup>23</sup> Further, levels of insulin receptor in GFAP-IGF-IR KO mice were normal (not shown). GFAP-IGF-IR KO mice were fertile, and food intake was also normal.

### Reagents

Anti-rabbit GFAP (1:1000) was obtained from DAKO (N0334), anti-chicken GFAP (1:1000) from ThermoFisher Scientific (PAI-10004), anti-rabbit Iba1 (1:1000) from WAKO (#019-19741), and anti-rabbit Aquaporin 4 (1:250) from Sigma (AB3594) were used. Anti-rabbit Alexa fluor 488, anti-rabbit Alexa fluor 647, and anti-chicken Alexa fluor 647 were used as secondary antibodies (ThermoFisher Scientific). Hoechst 33342 was purchased from Invitrogen (USA). 2,3,5-triphenyltetrazolium chloride (TTC) was purchased from Sigma (93140). Mouse/Rat IGF-I Quantikine ELISA Kit from R&D systems (MG100) was used to measure IGF-I in serum, according to manufacturer's protocol.

### Brain ischemic hemorrhage

This type of ischemic lesion is less frequent than the thrombotic type (around 15% of the total), and has a poorer prognosis.<sup>26</sup> We followed previously reported methods to reproduce it in mice, with modifications.<sup>27</sup> In brief, 6 to 9 months old mice (4–6 per group, both sexes) were anesthetized with 3% isoflurane (in O<sub>2</sub>) for induction and with 2% isoflurane for maintenance.

Rectal temperature was maintained at 36.5°C with a heating pad. An incision perpendicular to the line connecting the lateral canthus of the left eye and the external auditory canal was made to expose and retract the temporalis muscle. A burr hole was drilled, and frontal and parietal branches of the MCA were exposed by cutting and retracting the dura. The frontal branch of the MCA was carefully disrupted. Following surgery, mice were returned to their cages, kept at room temperature and allowed free access to food and water. All physiological parameters measured: rectal temperature, mean arterial pressure and blood glucose levels were not different between groups. At various times after surgery, MRI, and SPECT/CT brain scans were performed, animals sacrificed and brains collected and processed for further analyses. Infarct volume was measured by TTC staining 7 days after ischemia. After preparing 1 cm thick brain sections, the size of the lesioned area in each TTC stained brain slice was measured and summed for quantification using ImageJ. Sham surgery was performed in control littermates. This procedure leads to a relatively modest lesion, without long-lasting functional impairments, which mimics micro-hemorrhages with low clinical impact in the short-term.

### *Magnetic resonance imaging (MRI)*

Brain ischemic damage was imaged by MRI 1 week after injury at 4.7 Teslas using a BIOSPEC BMT 47/40 (Bruker, Germany), equipped with a 12 cm actively shielded gradient system. Mice were anaesthetized and injected intraperitoneally with 0.4 mmol/kg Gadopentetate dimeglumine (Gadolinium, Magnevist, Germany). Mice were put in prone position inside a cradle to avoid unexpected movements. A respiration sensor was used to survey the animal's vital functions. First, we acquired T2 weighted images using a fast spin echo sequence. The acquisition parameters were: TR = 4000 ms, effective TE = 60 ms, FOV = 3 cm, slice thickness = 1 mm and matrix = 256 × 192. This matrix size was increased during reconstruction by a zero-filling process in order to obtain images of 256 × 256 pixels. After that, weighted spin echo images were acquired (TR/TE = 700/15 ms) using the same geometrical parameters as above. These images were used to calculate injury volume using ParaVision software (Bruker, Germany). All comparative studies between controls and experimental groups were performed at 1 week after injury since at this time we observed largest lesion sizes.

### *Blood-brain-barrier (BBB) imaging*

BBB integrity was analyzed using SPECT imaging with <sup>99</sup>Tc-DTPA

(Tc-DTPA; 900 μCi) 2 days after cerebral ischemia. Mice were iv injected with <sup>99</sup>Tc-DTPA while awake and after 30 min of distribution of the tracer, they were imaged under anesthesia (2% isoflurane in O<sub>2</sub>), for 30 min (60 projections of 60 sec each), followed by CT acquisition (10 min), by means of an Albira II system (Bruker, Germany). SPECT and CT images were co-registered, reconstructed and analyzed. In normal conditions, the radiotracer is retained in the blood vessels, and it is only observed when the BBB is compromised. After fusion of both SPECT and CT images using the RM template Y.Uma, where the brain regions are outlined, images were masked for analysis of the volume presenting BBB disruption, to eliminate activity outside the brain (surgical damage). On those images, the activity to define the threshold was selected from the activity histogram. Then, the image was segmented by applying the "connected threshold", localizing an initial "seed" where the maximal activity value is located, by the PMOD software v 3.3 (Bruker, Germany). The volume of interest (VOI) was outlined and copied to analyze the contralateral non-ischemic side of the brain, then both volumes (ischemic and that on the contralateral side) and the activity therein were assessed. The experimenter was blind to the mice condition.

### *Sensorimotor function*

The adhesive removal test was performed 7 days after lesion as described.<sup>28</sup> In brief, prior to lesion, we performed a protocol of adhesive removal training during 5 days, twice a day. Mice were familiarized to the testing room at least 30 min before starting the experiment to allow habituation to the new environment. Thereafter, animals were removed from their home cages and one adhesive tape strip was applied on each paw with equal pressure. Mice were placed in the testing box and animal's behavior was observed. The time required to remove the tape strip from each paw was measured. Modified neurological severity scoring was performed 1 day after lesion, as described in detail elsewhere.<sup>29</sup> Motor, sensory, and reflex responses were graded on a scale of 0 (normal) to 14 (maximal deficit).

### *Immunocytochemistry*

Immunostaining was performed as described.<sup>30</sup> Animals were deeply anesthetized with pentobarbital and transcardially perfused with 4% paraformaldehyde in 0.1 M phosphate buffer, pH 7.4 (PB). Sagittal 50-μm thick sections were cut in a vibratome and collected in PB. Free-floating brain sections were blocked with 5% normal horse serum and incubated overnight at 4°C

with the respective primary antibody in PB containing 0.1% bovine albumin, 3% horse serum, and 0.2% Triton X-100. After several washes in PB, sections were incubated with an Alexa-coupled secondary antibody (1:1000) and analyzed in a Leica microscope. Using a 20× objective, the ischemic border region of each animal was imaged in 2 slices, 1 field per slice. A total of 8 images were used for analysis. The diameter of cerebral blood vessels profiled by AQP4 staining was measured with a 40× objective. A total of 8 images were used for analysis, 3 diameters per slice. Omission of primary antibody was used as control. Four mice were used for each experiment.

### RNA sequence analysis

Cortical regions from ischemic GFAP-IGF-IR KO mice and littermates were dissected and total RNA isolated using Trizol Reagent and RNeasy mini kit (Qiagen). RNA was recovered in RNase free water (Ambion). Quantification and Quality assessment was performed using nanodrop (ThermoFisher) and RNA integrity was evaluated by vertical electrophoresis (HS RNA cartridge, Bioptic SL). Only RNA samples with a RQ higher than 7 were used for posterior analysis. Libraries were prepared using TruSeq Total RNA Library prep (Illumina, Inc) and sequenced using NovaSeq6000 (Illumina, Inc) following a Pair End (2 × 120bp) protocol. Only samples with a Coverage QC > 85% were considered as valid for analysis. NGS data were analyzed using R-based algorithms. First reads quality was assessed using FastQC tool. Sequence alignment was performed using Hisat2, and reads counting and differential expression analysis was performed using DESeq2. The Benjamini-Hochberg method of correction was established as the p-value adjustment method. Any gene with q-value < 0.05 was considered as statistically significant, and as a differentially expressed gene (DEG). The R packages clusterProfiler and enrichplot were used to perform the Over Representation Analysis (ORA). The Gene Ontology (GO) knowledgebase was used as the background database, the Benjamini-Hochberg method of correction was set as the p-value adjustment method and the q-value cutoff at 0.05.

### Quantitative PCR

Total RNA isolation from cell lysates or brain tissue was carried out with Trizol. One µg of RNA was reverse transcribed using High Capacity cDNA Reverse Transcription Kit (Life Technologies) according to the manufacturer's instructions. For the quantification of specific genes, total RNA was isolated and transcribed as above, and 62.5 ng of cDNA was

amplified using TaqMan probes for vascular endothelial growth factor alpha (*Vegfα*) and *18S* as endogenous control (Life Technologies), and SYBR green probes for *cd93*, Platelet And Endothelial Cell Adhesion Molecule 1 (*pecam1*), tenascin-C (*tnc*), *Igf1*, early growth response protein 1 (*Egr1*), C-C Motif Chemokine Ligand 2 (*Ccl2*), nerve growth factor (*Ngf*), fibroblast growth factor 2 (*Fgf2*), brain-derived neurotrophic factor (*Bdnf*), aquaporin 4 (*Aqp4*), Complement C1q A Chain (*C1qa*) and glyceraldehyde-3-phosphate dehydrogenase (*Gapdh*) as endogenous control (Life Technologies). Each sample was run in triplicate in 20 µl of reaction volume using TaqMan Universal PCR Master Mix according to the manufacturer's instructions (Life Technologies) or SYBR green Master Mix according to the manufacturer's instructions (Life Technologies). All reactions were performed in a 7500 Real Time PCR system (Life Technologies). Quantitative real time PCR analysis was carried out as previously described.<sup>31</sup> Results were expressed as relative expression ratios on the basis of group means for target transcripts versus reference transcript. All SYBR primers were designed by Sigma Aldrich (see Suppl. Table 1), and Taqman primers were designed by ThermoFisher Scientific. At least three independent experiments were done.

### Statistical analysis

Statistical analyses were carried out using GraphPad Prism 5 software or JMP 14 software. The Kolmogorov-Smirnov test was used to check if the groups followed a normal distribution. If all groups passed the normality test, then we used one-way ANOVA followed by Bonferroni's multiple comparison test. If the groups did not pass the normality test, we used a non-parametric Mann-Whitney test for comparing 2 groups, and the Kruskal-Wallis test (with the Dunn's multiple comparison test as post-hoc) for more than two groups. Graphs depict mean value ± standard deviation (SD) and the *p* values shown are coded as follows: \**p* < 0.05, \*\**p* < 0.01, \*\*\**p* < 0.001.

## Results

### Astrocytic IGF-I receptor-deficient mice are more vulnerable to ischemic hemorrhage

Since astrocytes participate in brain responses to ischemia<sup>32</sup> and astrocytic IGF-I has been shown to promote protection against stroke insult,<sup>33</sup> we determined whether its receptor in this type of glial cell play a role in the response to ischemic damage. We used Cre/Lox mice where ablation of the IGF-IR in astrocytes was driven by tamoxifen (GFAP-IGF-IR

KO mice). Ischemic injury in these mice was significantly larger one week after insult than control littermates, as determined by MRI analysis (Figure 1(a) and (b)). Increased lesion volume in GFAP-IGF-IR KO mice was histologically confirmed with 2,3,5-triphenyl-tetrazolium chloride (TTC) stainings (Figure 1(c)). The area under the curve of the unstained area, as determined by absence of TTC staining, was significantly larger than in littermates: GFAP-IGF-IR KO:  $7.68 \pm 2.40 \text{ mm}^2$  vs control littermates:  $2.68 \pm 2.64 \text{ mm}^2$ ,  $p < 0.05$  (Figure 1(d)). The effect was specific for IGF-IR since elimination of the closely related insulin receptor (IR) in astrocytes using a similar tamoxifen-regulated GFAP-IR KO model<sup>25</sup> showed no obvious change in the ischemic area (Suppl Figure 2A,B).

Injured GFAP-IGF-IR KO mice also show increased BBB disruption, as determined by <sup>99m</sup>Tc-DTPA SPECT/CT imaging (Figure 2(a)). Two days after ischemic insult, mean uptake of the tracer in the ipsilateral side of the brain was significantly higher in GFAP-IGF-IR KO mice, as compared to control littermates with one-way ANOVA: GFAP-IGF-IR KO:  $0.983 \pm 0.149$  vs control littermates:  $0.764 \pm 0.141 \text{ mm}^2$ ,  $p < 0.05$  (Figure 2(b)). However, at this early time, SPECT/CT analysis did not detect changes in the ischemic volume between experimental groups (Suppl Figure 2C).

### Functional impact of down-regulation of astrocytic IGF-IR activity

The functional impact of ischemic injury, assessed by two tests, varied according to observed changes in lesion size. Thus, increased lesion size was reflected in greater neurological deficits; neurological severity scale in GFAP-IGF-IR KO was 6 score 3, 4 score 2 vs 3 score 2, 3 score 1, 1 score 0 in control littermates;  $p < 0.01$  (Figure 3(a)). As expected, injured control mice showed five times higher neurological severity score than littermates after sham surgery. Furthermore, one week after ischemic insult, mean time to remove the tape from the affected right paw in the adhesion removal test was longer in GFAP-IGF-IR KO mice than in control littermates (Mann-Whitney test): GFAP-IGF-IR KO:  $191.8 \pm 118.2 \text{ sec}$  vs control littermates:  $29.2 \pm 26.8 \text{ sec}$ ,  $p < 0.05$  (Figure 3(b)), reflecting poorer sensorimotor coordination. At this time after lesion, no changes in removal time were observed between control and littermates after sham surgery (Figure 3(b)), indicating that the functional impact in control injured animals is short-lasting.

After ischemic surgery, we observed increased gene expression of IGF-I in the ipsilateral cerebral cortex of injured control mice as compared to sham surgery mice, and even greater increased expression in injured

GFAP-IGF-IR KO mice: GFAP-IGF-IR KO:  $3.76 \pm 1.22$  vs control littermates:  $2.25 \pm 0.97 \text{ sec}$ ,  $p < 0.01$  (Figure 3(c)). In parallel, serum IGF-I levels significantly decreased in both GFAP-IGF-IR KO and littermates after ischemic surgery (Figure 3(d)). This was paralleled by smaller weight gain in these groups (Suppl Figure 2D).

### Peri-lesion cellular and molecular adaptations to reduced astrocyte IGF-IR activity

Under pathological conditions such as ischemia, astrocytes and other glial cells secrete inflammatory signals compromising BBB integrity.<sup>34</sup> Injured brains were collected for RNAseq gene expression analysis 3 days after surgery, when the expression of various inflammatory cytokines peaks.<sup>35–37</sup> The results show 22 known up- or down differentially regulated genes (DEGs) in GFAP-IGF-IR KO mice compared to controls with a q-value  $< 0.05$  and a fold change  $> 0.5 \text{ Log}^2$  (Figure 4(a)). Variability in expression levels of these 22 DEG show that control and GFAP-IGF-IR KO samples clustered depending only on genotype (Figure 4(b)). Gene ontology analysis (Figure 4(c)) indicated that the majority of DEG expressed in GFAP-IGF-IR KO mice were related to regulation of the inflammatory response (3 from 22 genes, fold enrichment 28), integrin cell surface integration (3 from 22 genes, fold change = 22.6), angiogenesis (4 from 22 genes, fold enrichment = 12.8), and cell-cell adhesion (4 from 22 genes, fold change = 17.8). Pathway analysis showed those related to extracellular matrix interaction, cholesterol metabolism, and other pathways related to immune responses such as malaria, ALS, and leukocyte migration, and finally to the PI3-AKT signaling pathway (Figure 4(d)). Collectively, the results indicate that the immune response in GFAP-IGF-IR KO mice was increased after ischemic damage.

A few selected genes of these pathways: Cd93, Pecam1, and Tnc, were confirmed by qPCR (Figure 5 (a) to (c)). We used the latter technique to examine expression of additional classical inflammatory factors known to be secreted by astrocytes and potentially affecting BBB integrity. Expression of Egr1, C1qa, Ccl2, and Aqp4 in the ipsilateral side of the cortex was significantly higher in GFAP-IGF-IR KO mice (Figure 5(d) to (g)) whereas the levels of various growth factors (Ngf, Fgf2, Bdnf, and Vegf $\alpha$ ) were not significantly altered (Suppl Figure 3).

Next, we investigated whether worsened functional and anatomical outcomes were associated with changes in glial reactivity, a key cellular component in brain inflammatory responses. Immunostaining of glial fibrillary acidic protein (GFAP) astrocytes and allograft inflammatory factor 1 (Iba1) microglia showed that GFAP+ astrocytes neighboring the lesion area in

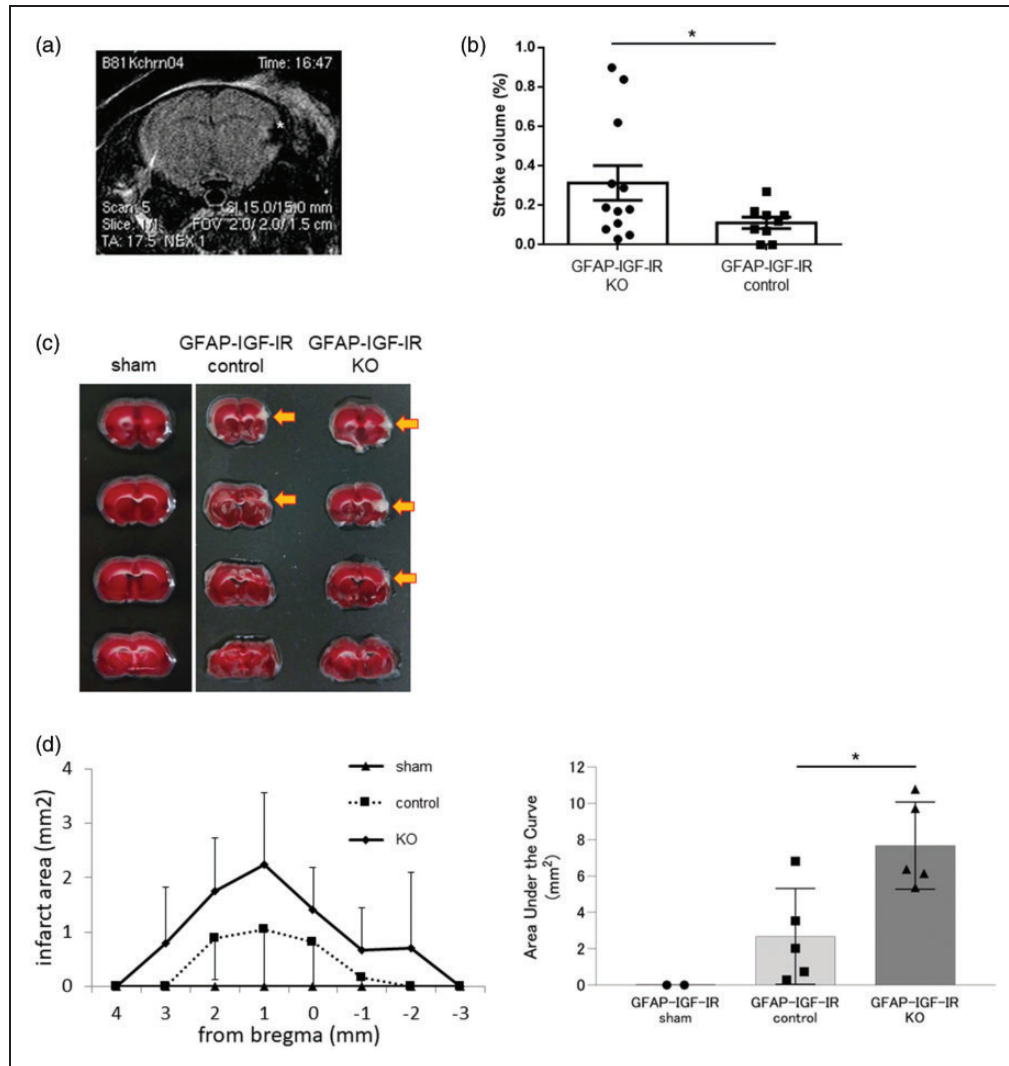


**Figure 1.** Reduced astrocytic IGF-IR activity and responses to ischemia. a, Representative brain magnetic resonance imaging (MRI); The asterisk shows the ischemic area. b, MRI evaluation of brain stroke volume in GFAP-IGF-IR KO mice ( $n = 9$ ) and GFAP-IGF-IR control littermates ( $n = 12$ ) ( $*p < 0.05$ ). c, Representative 2,3,5-triphenyltetrazolium chloride (TTC) staining in injured GFAP-IGF-IR KO and GFAP-IGF-IR littermates and in sham GFAP-IGF-IR littermates; arrowhead shows the ischemic area. d, Left: infarct area determined by TTC staining 7 days after surgery along the anterior-posterior axis in lesioned (GFAP-IGF-IR KO mice  $n = 5$ , and GFAP-IGF-IR littermates,  $n = 5$ ), and sham-operated GFAP-IGF-IR littermates ( $n = 2$ ). Position of coronal sections relative to bregma is indicated in the X axis. Right bars: lesion volume calculated as area under the curve for each respective group (control vs. KO;  $p = 0.047$ ).

GFAP-IGF-IR KO mice were as abundant as in control littermates in number but show distinct morphological features (Figure 6(a)). Thus, the number of polarized GFAP<sup>+</sup> astrocytes with cytoplasmic extensions towards the lesion, that are considered to eventually form the peri-lesion scar,<sup>38</sup> was significantly higher in littermates: GFAP-IGF-IR KO:  $227.67 \pm 98.50$  count/mm<sup>2</sup> vs control littermates:  $366.36 \pm 68.20$  count/mm<sup>2</sup>,  $p < 0.01$  (Figure 6(b)), while the number of stellated astrocytes was significantly higher in GFAP-IGF-IR-KO mice: GFAP-IGF-IR KO:  $398.64 \pm 148.79$  count/mm<sup>2</sup> vs control

littermates:  $242.50 \pm 116.60$  count/mm<sup>2</sup>,  $p < 0.05$  (Figure 6(b)). Furthermore, Iba1<sup>+</sup> microglia within 300  $\mu$ m of the lesion area in GFAP-IGF-IR KO mice show an altered distribution (Figure 6(c)). Iba1<sup>+</sup> cells positioned in the proximal part of the lesion area, that is thought to be important in preventing spread of the injury,<sup>39</sup> were comparatively reduced in GFAP-IGF-IR KO mice. Thus, microglia was widely distributed in the more distal part of the lesion in KO mice. As a result, the proximal/distal distribution of Iba1<sup>+</sup> microglia differed in GFAP-IGF-IR KO mice, compared to control littermates.

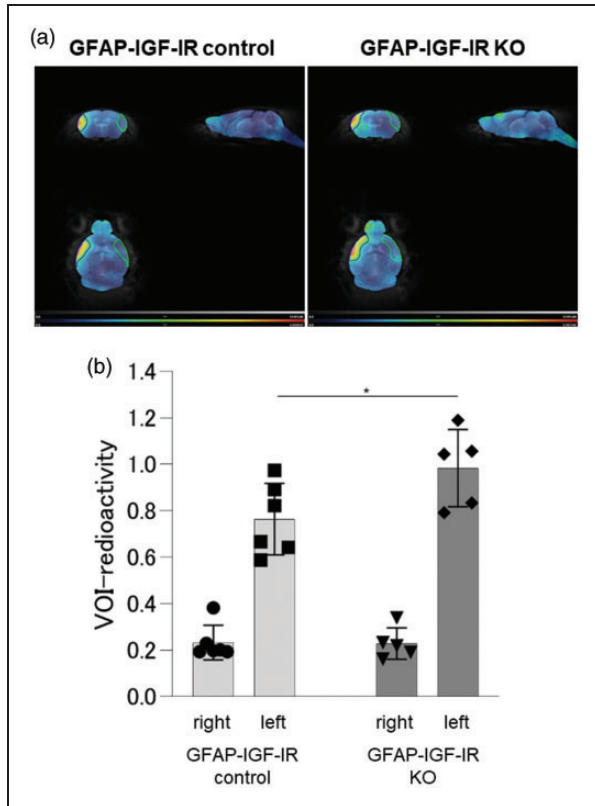


**Figure 2.** Reduced brain IGF-IR activity and BBB integrity. a, Representative SPECT/CT imaging with  $^{99m}\text{Tc}$ -diethylene-triamine-pentaacetate (Tc-DTPA); the outlined area is a volume of interest (VOI) and copied to analyze the contralateral non-ischemic side. b, Evaluation of the radioactivity by  $^{99m}\text{Tc}$ -DTPA SPECT in GFAP-IGF-IR KO mice ( $n=5$ ) and GFAP-IGF-IR control littermates ( $n=6$ ) (control left vs. KO left;  $p=0.049$ ). Radioactivity is expressed as % injected dose/cc.

In addition, we examined the cellular distribution of aquaporin (AQP) 4, which is present in astrocytic endfeet contacting cerebral vessels,<sup>40</sup> since increased AQP expression is associated with exacerbation of cerebral edema during brain injury.<sup>41</sup> We could not find a clear difference in the distribution of AQP4+ cells in GFAP-IGF-IR KO mice as compared to their GFAP-IGF-IR controls (Figure 7(a)), although the AQP4+ area around the lesion site was significantly larger in GFAP-IGF-IR KO mice than in littermates (GFAP-IGF-IR controls): GFAP-IGF-IR KO:  $0.185 \pm 0.086$  area/ $\text{mm}^2$  vs control littermates (GFAP-IGF-IR controls):  $0.096 \pm 0.047$  area/ $\text{mm}^2$ ,  $p < 0.001$  (Figure 7(b)). Regarding the vessel diameter determined by AQP4 staining, no changes were observed in GFAP-IGF-IR KO mice compared to GFAP-IGF-IR controls; GFAP-IGF-IR KO:  $6.619 \pm 1.178$   $\mu\text{m}$  vs GFAP-IGF-IR controls:  $6.389 \pm 0.590$   $\mu\text{m}$ ,  $p = 0.633$  (Suppl Figure 4).

## Discussion

These results indicate that the activity of the astrocytic IGF-IR, but not of the closely related insulin receptor, is essential in responses to hemorrhagic ischemia as its absence produces greater tissue damage and more pronounced functional impairment. Thus, as already suggested for astrocytes in general,<sup>42</sup> enhancement of IGF-IR activity in this type of glial cells may prove a beneficial strategy for hemorrhagic ischemia. Of note, reduced IGF-IR activity in neurons was previously shown to diminish damage after stroke,<sup>23</sup> suggesting either lesion-specific or cell autonomous actions of brain IGF-IR in the response to insult. Diverse observations may help clarify these potentially conflicting results.

Neuronal IGF-IR deficient mice showed a phenotype that is quite different from GFAP-IGF-IR KO mice.<sup>23</sup> The former show body overgrowth and high serum IGF-I levels, whereas the latter has these parameters within normal range. As indicated by the authors, neuronal IGF-IR deficient mice may show increased neuroprotection through increased availability of IGF-I at the lesion site.<sup>23</sup> Thus, defective IGF-IR signaling in astrocytes seems a key difference between the two types of mice. Indeed, when IGF-I signaling was specifically knocked down in astrocytes by using the tamoxifen-regulated strategy (similar to the one used to produce neuronal-specific mutants), lesion size after hemorrhagic stroke was aggravated, while these mutant mice had normal body weight and unaltered serum IGF-I levels. Central and peripheral changes according to brain cell type where IGF-IR activity is modified, reinforce the notion of cell-specific actions of IGF-I.

The present observations suggest that cell autonomous actions of IGF-IR in brain cells may play varied roles in neuroprotection. Whereas opposite responses to ischemic damage between mice with reduced IGF-IR in neurons,<sup>23</sup> and mice with reduced IGF-IR in astrocytes (present findings) could be attributed to differences in the type of experimental ischemia used in each study, reducing IGF-IR activity in neurons protects not only against ischemia, but also against AD and spino-motor pathologies,<sup>43-45</sup> making neuronal IGF-IR detrimental to responses to other types of tissue damage. Of note, since elimination of IGF-IR activity in astrocytes was sufficient to worsen responses to ischemia, a possible use of drugs blocking IGF-IR activity regardless of cell type for brain diseases,<sup>46</sup> should be reconsidered. Moreover, the presence of IGF-IR in specific cellular compartments in glia<sup>47</sup> and neurons (in preparation), mediating complex neuronal plasticity patterns, at least in the latter,<sup>48,49</sup> suggests the existence of a highly compartmentalized role of this growth factor and its receptor on brain function.

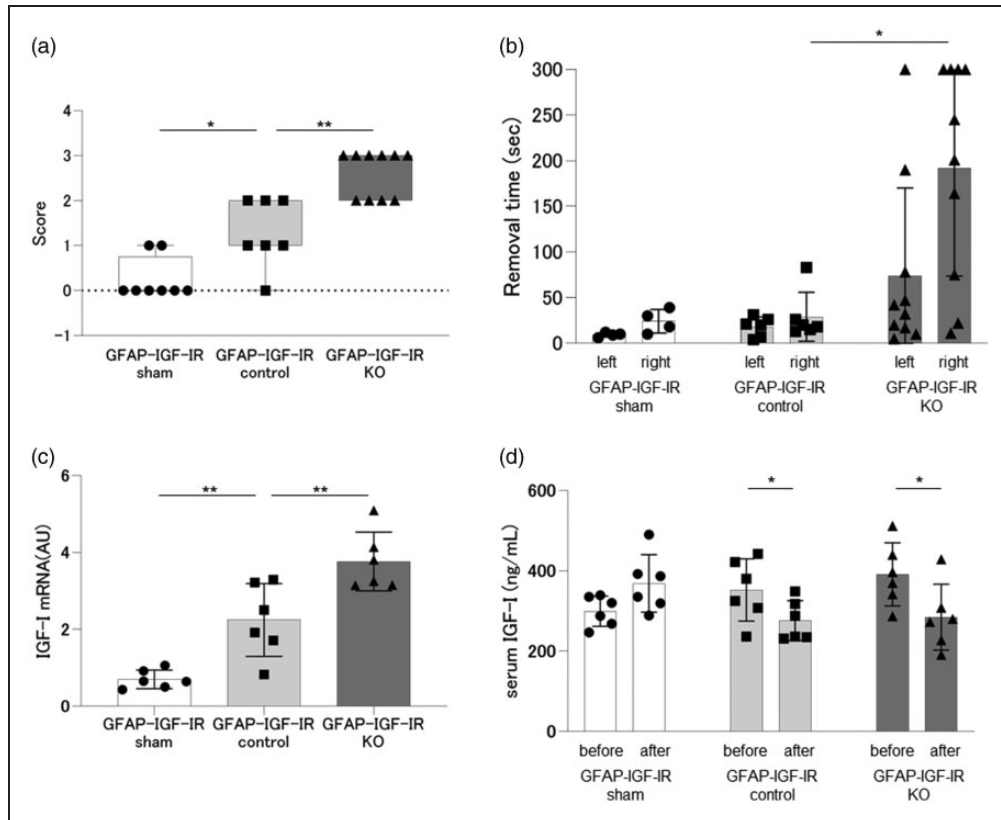


**Figure 3.** Functional impact of deletion of IGF-IR in astrocytes. (a) Neurological severity score in GFAP-IGF-IR KO mice ( $n = 10$ ), GFAP-IGF-IR control littermates ( $n = 7$ ) (control vs. KO;  $p = 0.006$ ), and GFAP-IGF-IR control littermates after sham surgery ( $n = 8$ ) (sham vs. control;  $p = 0.003$ ). (b) Ipsilateral sensorimotor function determined by the adhesive removal test in GFAP-IGF-IR KO mice ( $n = 10$ ), GFAP-IGF-IR control littermates ( $n = 6$ ), and GFAP-IGF-IR control littermates after sham surgery ( $n = 4$ ) (control right vs. KO right;  $p = 0.022$ ). (c) IGF-I mRNA levels in ipsilateral cortex of GFAP-IGF-IR KO mice ( $n = 6$ ), GFAP-IGF-IR control littermates ( $n = 6$ ) (control vs. KO;  $p = 0.010$ ), and GFAP-IGF-IR control littermates after sham surgery ( $n = 6$ ) (sham vs. control;  $p = 0.003$ ) and (d) Serum IGF-I levels before and after injury; serum samples were collected from GFAP-IGF-IR KO ( $n = 6$ ) (KO before vs. after surgery;  $p = 0.045$ ), GFAP-IGF-IR control littermates before/after surgery (control before vs. after surgery;  $p = 0.014$ ), and GFAP-IGF-IR control littermates ( $n = 6$ ) before/after sham surgery.

Indeed, neuroprotection by IGF-I against stroke differs when this growth factor is administered intra-cerebroventricularly,<sup>16</sup> than when is overexpressed in astrocytes in the infarct area.<sup>33</sup> As a corollary, the role of IGF-IR in other types of brain cells in the response to injury should be examined, as suggested recently.<sup>50</sup> For instance, it cannot be excluded that IGF-IR in microglia<sup>23</sup> and brain endothelium<sup>20,51</sup> will play an important role in the response to stroke insult, as it is widely over-expressed in the region surrounding the lesion.<sup>52</sup> Recent data reinforce the need to separately analyze a possible differential role of IGF-IR in astrocytes and microglia in the response to stroke.<sup>53</sup>

GFAP-IGF-IR KO mice showed cellular and molecular changes after ischemia compatible with aggravated responses to damage. Firstly, there was increased expression of a total of 20 genes involved in inflammatory, cell-adhesion and angiogenic pathways, which

likely reflects potentiation of these putatively protective mechanisms. In particular, Cd93, which is involved in cell adhesion and clearance of apoptotic cells,<sup>54</sup> Pecam1, a member of the immunoglobulin superfamily whose expression increases due to BBB disruption,<sup>55</sup> and Tnc, which is involved in neurogenesis,<sup>56</sup> are up-regulated in GFAP-IGF-IR KO mice. In general, brain IGF-I protein increased 2-7 days after surgery,<sup>57</sup> and we collected mRNA 3 days after surgery to see the changes. However, abundant evidence points to complex patterns and timing of reparative responses after brain trauma, making it difficult to establish a direct link between these changes and the observed up-regulated genes. Additional limitations of our study are the lack of time-course analysis of molecular changes and the lack of comparison between male and female mice. The latter is particularly relevant, as sex-dependent responses to stroke are well documented.<sup>58,59</sup>



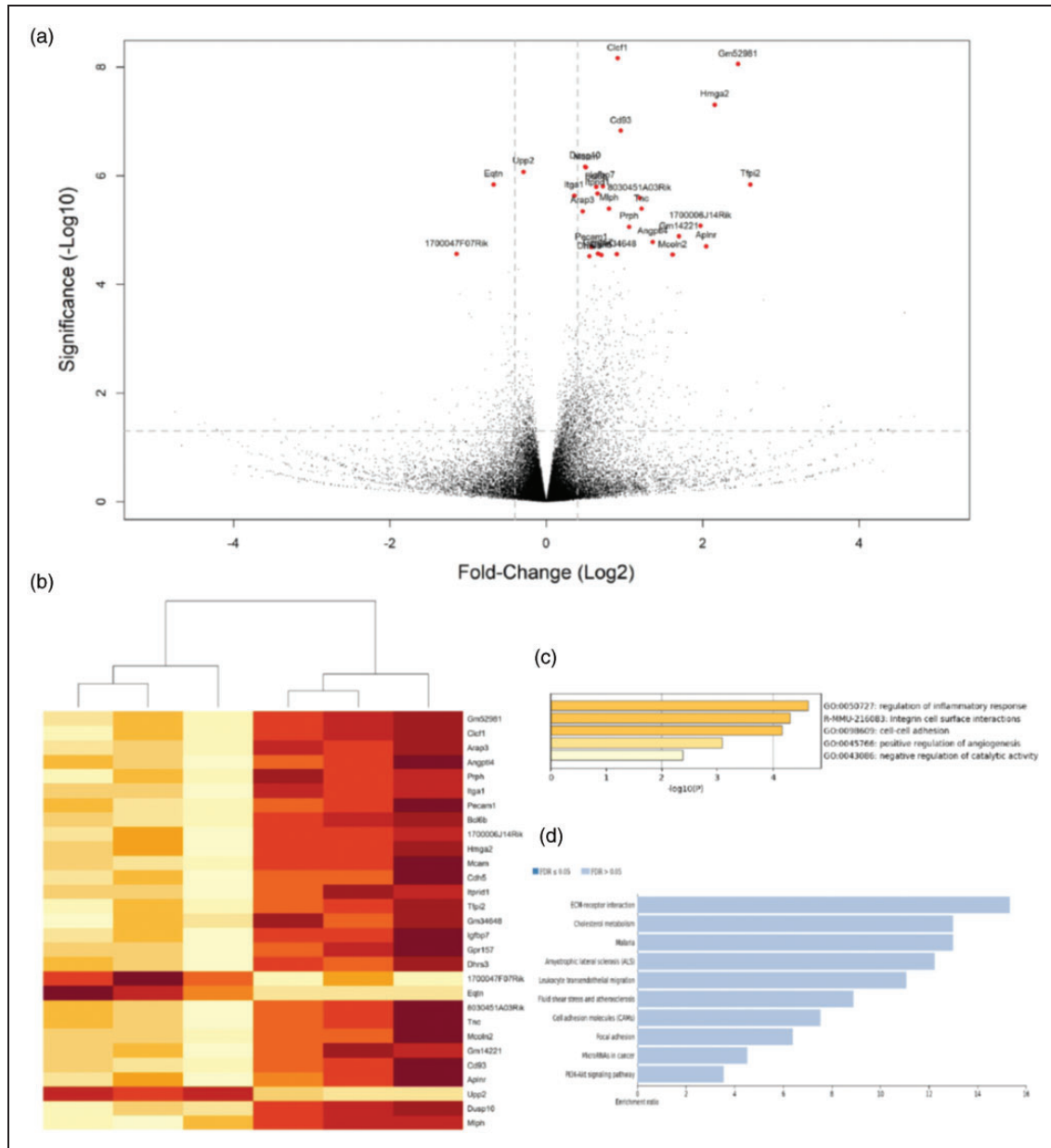


**Figure 4.** Transcriptional landscape after deletion of IGF-IR in astrocytes. (a) Volcano plot showing differentially expressed genes between GFAP-IGF-IR KO mice and control littermates. (b) Heatmap analysis of differentially expressed genes. (c) Gene ontology analysis of differentially expressed genes and (d) Gene ontology enrichment analysis of differentially expressed genes.

Importantly, astrocyte-dependent mechanisms in relation to sex-specific responses to stroke have already been reported to involve female differences in stroke-induced inflammation.<sup>60</sup> Thus, future studies should focus on providing time- and sex-dependent information in this model.

In turn, reactive astrocytes in control mice showed elongated cytoplasmic extensions towards the lesion core 7 days after injury, while in GFAP-IGF-IR KO mice, astrocytes show a stellate morphology corresponding to an earlier, acute phase (1–4 days) of

the process,<sup>38</sup> suggesting a delayed/impaired response. Although the role of reactive glia after brain injury remains controversial,<sup>61–64</sup> our observations indicate that morphological changes in reactive astrocytes lacking IGF-IR are associated to greater damage, suggesting that cellular interactions in the penumbra environment (probably directed to scar formation) are important modulators of post-injury responses.<sup>65</sup>

Activated microglia in the ischemic brain is recruited to the penumbra region and is thought to prevent the spread of inflammation via phagocytosis of dead

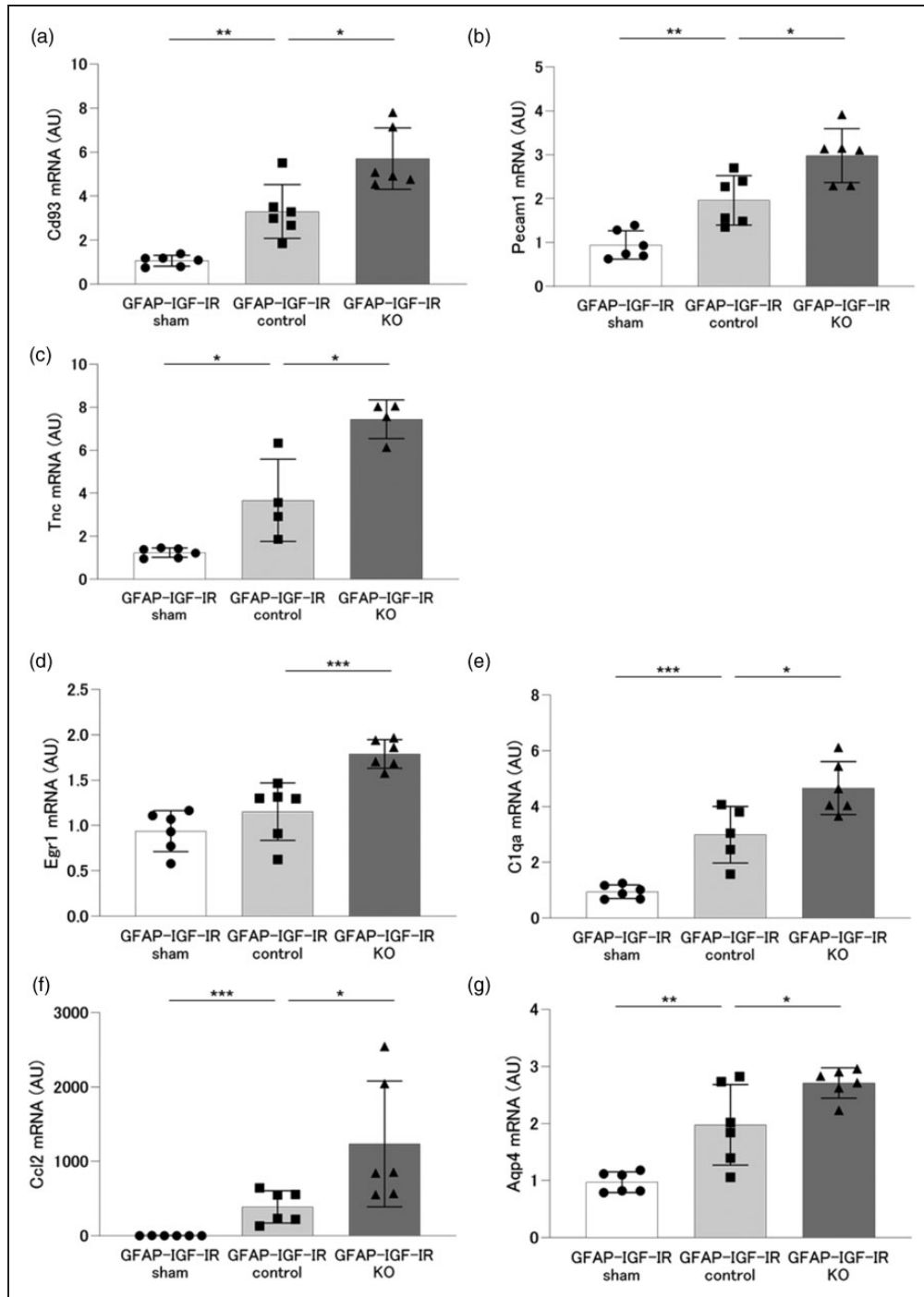


**Figure 5.** Molecular impact of IGF-IR deletion in astrocytes. (a) mRNA levels of Cd93 (sham vs. control;  $p = 0.001$ , control vs. KO;  $p = 0.010$ ). (b) Pecam1 (sham vs. control;  $p = 0.003$ , control vs. KO;  $p = 0.013$ ). (c) Tnc (sham vs. control;  $p = 0.013$ , control vs. KO;  $p = 0.012$ ). (d) Egr1 (sham vs. control;  $p = 0.207$ , control vs. KO;  $p = 0.001$ ). (e) C1qa (sham vs. control;  $p = 0.001$ , control vs. KO;  $p = 0.020$ ). (f) Ccl2 (sham vs. control;  $p = 0.001$ , control vs. KO;  $p = 0.039$ ). (g) Aqp4 (sham vs. control;  $p = 0.007$ , control vs. KO;  $p = 0.038$ ) in ipsilateral cortex of GFAP-IGF-IR KO mice ( $n = 6$ ), GFAP-IGF-IR control littermates ( $n = 6$ ), and GFAP-IGF-IR control littermates after sham surgery ( $n = 6$ ). \* $p < 0.05$ , \*\* $p < 0.01$  and \*\*\* $p < 0.001$  vs respective controls.

nerves.<sup>39</sup> In GFAP-IGF-IR KO mice, microglia could potentially be more strongly recruited to the lesion site by higher local levels of Ccl2, which is predominantly secreted by astrocytes,<sup>66</sup> but this was not the case;

microglia in mutant mice was more abundantly present distal to the lesion site. We hypothesize that increased expression of C1qa, a microglial cytokine which contributes to phenotypic conversion of astrocytes into a

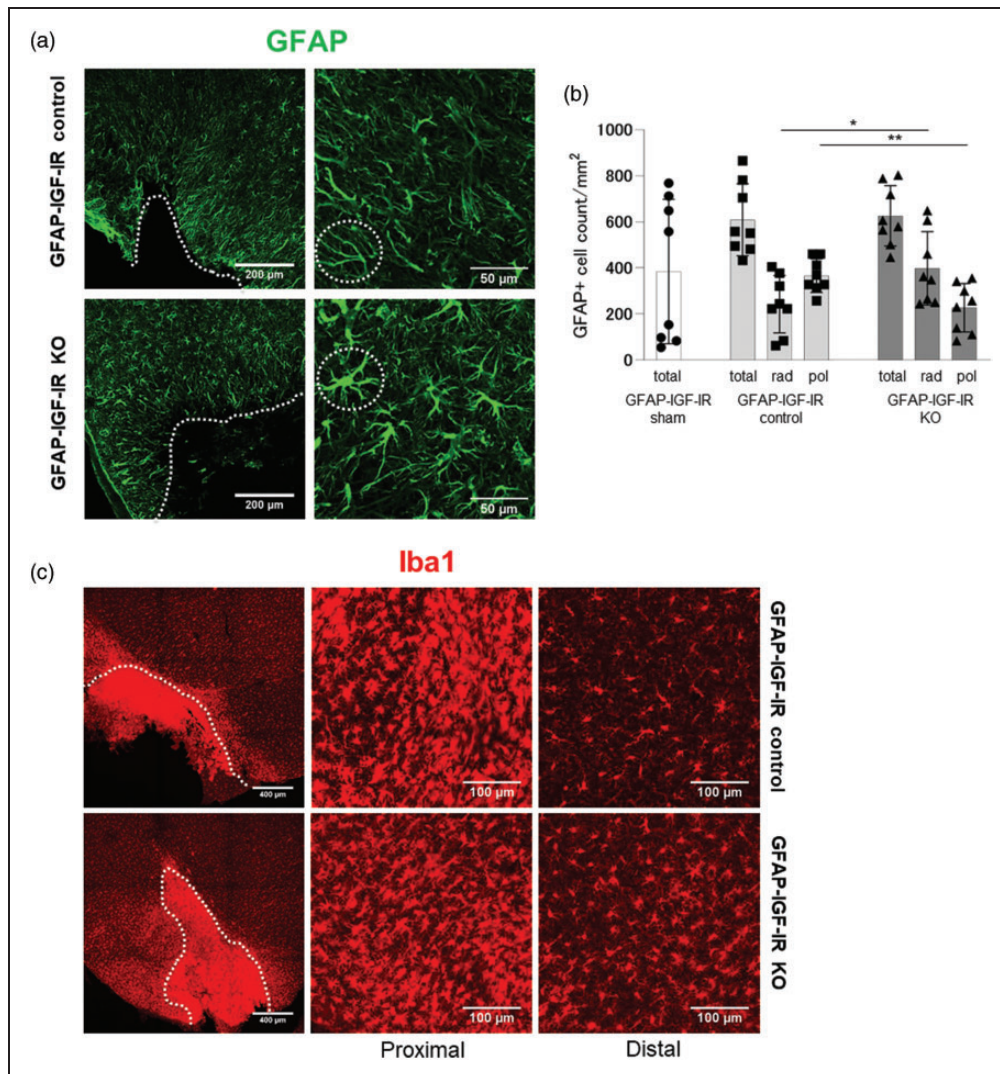


**Figure 6.** Differential morphological features in reactive astroglia and in microglia distribution in GFAP-IGF-IR KO mice after ischemic injury. (a) Left: representative low magnification images of GFAP immune-stained cells in GFAP-IGF-IR KO mice and GFAP-IGF-IR control littermates; dashed lines indicate the position of the ischemic lesion. Right: Higher-power images of GFAP+ cells to illustrate the distinct morphology: polarized cells in littermates and radial shapes in GFAP-IGF-IR KO mice. Representative cell morphologies are surrounded by dotted lines. (b) Evaluation of the number of GFAP+ cells with polarized elongated cytoplasm and radial morphology in GFAP-IGF-IR KO mice ( $n = 8$ ), GFAP-IGF-IR control littermates ( $n = 8$ ) (radial control vs. KO;  $p = 0.046$ , polarized control vs. KO;  $p = 0.008$ ), and GFAP-IGF-IR control littermates after sham surgery ( $n = 8$ ) and (c) Left: low magnification immunostaining of Iba1+ cells in GFAP-IGF-IR KO and GFAP-IGF-IR control littermates; Center and right panels: higher magnification illustrating distribution of Iba1+ cells within 300  $\mu\text{m}$  (proximal) and beyond 300  $\mu\text{m}$  (distal) from the lesion site, respectively. The white dotted line indicates the ischemic site.

neurotoxic subtype,<sup>67</sup> may distort microglia recruiting. Microglia has neuroprotective effects in the acute phase of stroke,<sup>68</sup> and microglia processes are necessary for the closure of the BBB.<sup>69</sup> Our observation indicates that altered recruiting of microglia is associated to greater damage, suggesting that prevention of inflammation spread is impaired.<sup>39</sup> Although further studies are needed to determine the mechanism by which activated microglia is not properly recruited to the vicinity of the lesion in the brain of GFAP-IGF-IR KO mice,

an additional possibility might involve *Egr1*, which is strongly expressed in astrocytes during ischemia.<sup>70</sup> *Egr1* KO rats show decreased ischemic damage, edema improvement, and decreased number of recruited microglia, while the ischemic area is increased in rats overexpressing *Egr1*.<sup>71</sup> In GFAP-IGF-IR KO mice, *Egr1* was highly expressed, so it can also contribute to altered distribution of microglia.

In GFAP-IGF-IR KO mice, expression of AQP4 was increased, as determined by both qPCR and

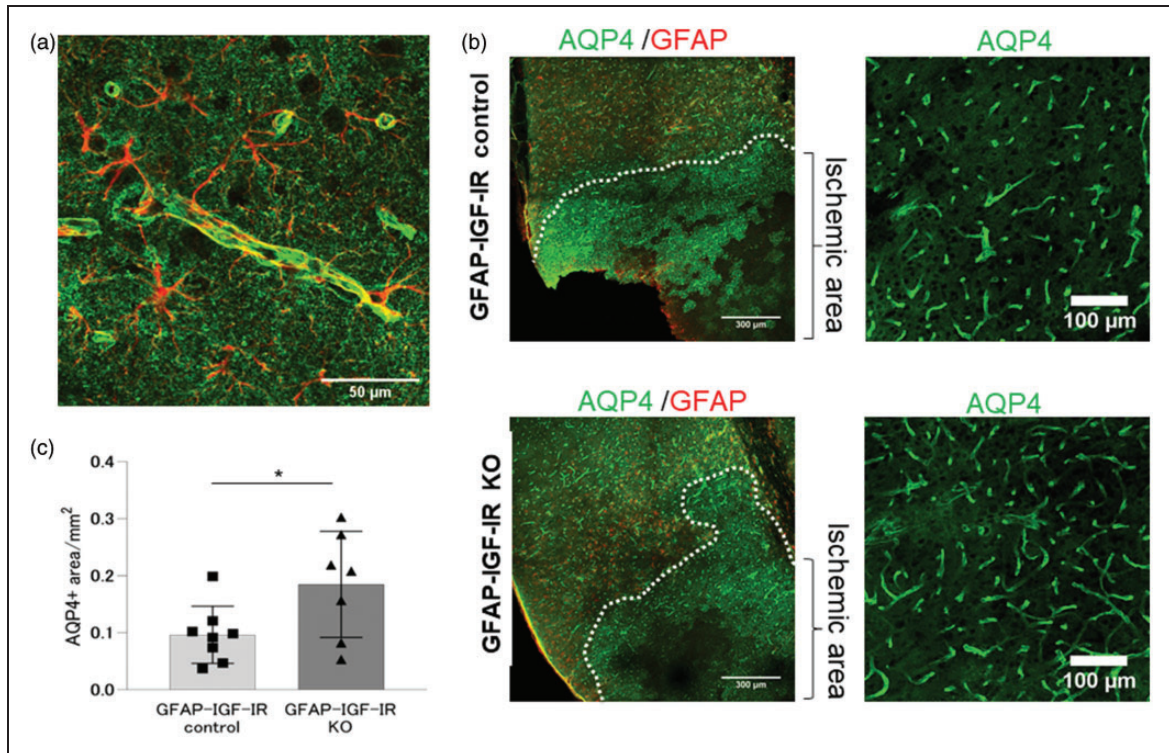


**Figure 7.** Aquaporin 4 expression in reactive astroglia of GFAP-IGF-IR KO mice after ischemic injury. (a) Representative double GFAP/AQP4 immunostaining illustrating expression of AQP4 in astroglial end-feet ensheathing brain vessels. (b) Immunostaining of AQP4+ area in GFAP-IGF-IR KO and GFAP-IGF-IR control littermates; the right figures show high-resolution image taken around the lesion site. The white dotted line is the ischemic site estimated from activated astroglia. (c) Evaluation of the AQP4+ area in GFAP-IGF-IR KO mice ( $n = 8$ ) and GFAP-IGF-IR control littermates ( $n = 8$ ;  $p = 0.036$ ).

immunostaining. AQP4 is a brain water channel affecting the evolution of cerebral edema after injury<sup>72</sup> and is expressed mainly on astrocyte end-feet around the brain vessels. Expression of AQP4 is increased not only in astrocyte end-feet but also throughout the entire astrocyte cells after 48 hours of ischemia.<sup>72</sup> While we did not observe a clear difference in the distribution of AQP4 after ischemic insult, we speculate that an increased proportion of astrocytes with radial shapes found in GFAP-IR KO mice may interfere with proper distribution of AQP4 in astrocytic end-feet and in this way hinder edema resolution. However, further analysis is needed. Astrocytes play an important role in controlling cerebral blood flow,<sup>73</sup> and previous reports have shown that the depolarization around the ischemic area and the contraction of smooth muscle cells after ischemia decrease the velocity of cerebral blood flow and increase the diameter of blood vessels.<sup>74,75</sup> However, we did not detect a role of astrocytic IGF-IR in cerebral blood flow, confirming previous observations.<sup>76</sup> Nevertheless, further analysis is warranted.

Collectively, these findings provide a nuanced view of the role of brain IGF-I signaling in the response to

ischemic insult, indicating that context- and cell-dependent actions of IGF-I need to be considered when analyzing its biological significance. Indeed, recent preliminary observations support a strong context-dependent role of IGF-I signaling in stroke, as time after stroke and type of stroke determine the role of IGF-IR in astrocytes.<sup>50</sup> These observations also support the use of targeted increase of IGF-IR activity in astrocytes as a therapeutic approach to improve resistance to ischemic injury. Indeed, these cells are important determinants of neurodegenerative processes,<sup>77</sup> and key mediators of neuroprotection after ischemia.<sup>78</sup> Therefore, strategies directed to this goal need to be developed. For example, physical exercise has been shown recently by us to increase total IGF-IR levels in mouse brain,<sup>79</sup> and physical activity has been proven to protect against stroke in humans.<sup>80</sup> It is possible that this protection involves the astrocytic IGF-IR.

#### Funding

The author(s) disclosed receipt of the following financial support for the research, authorship, and/or publication of this article: This work was funded by Cibernet (Instituto de Salud

Carlos III, Spain) and CAM NEUROMETAB-CM (B2017/BMD-3700).

### Acknowledgements

We are thankful to M. Garcia and L Guinea for technical support and to the Omics Technologies Laboratory of the Cajal Institute.

### Declaration of conflicting interests


The author(s) declared no potential conflicts of interest with respect to the research, authorship, and/or publication of this article.

### Authors' contributions

KS design and performed experiments, analyzed and graphed the results and wrote parts of the manuscript, JP performed experiments, LG performed experiment and analyzed and prepared results, AMF, EFdeS, IFdeC, AP-R, MLdeC, and SD-P, performed experiments, RH-L performed experiments and prepared results; ITA designed and coordinated the study, and wrote the manuscript.

### ORCID iDs

Estrella Fernandez de Sevilla  <https://orcid.org/0000-0002-2693-1861>

Ignacio Torres Aleman  <https://orcid.org/0000-0001-8107-7947>

### Supplementary material

Supplemental material for this article is available online.

### References

- Dolgin E. To serve and neuroprotect. *Nat Med* 2012; 18: 1003–1006.
- Bam K, Olaiya MT, Cadilhac DA, et al. Enhancing primary stroke prevention: a combination approach. *Lancet Public Health* 2022; 7: e721–e724.
- Fisher M and Saver JL. Future directions of acute ischemic stroke therapy. *Lancet Neurol* 2015; 14: 758–767.
- Albers GW, Marks MP, Kemp S, et al. Thrombectomy for stroke at 6 to 16 hours with selection by perfusion imaging. *N Engl J Med* 2018; 378: 708–718.
- Joy MT and Carmichael ST. Encouraging an excitable brain state: mechanisms of brain repair in stroke. *Nat Rev Neurosci* 2021; 22: 38–53.
- Wahl AS and Schwab ME. Finding an optimal rehabilitation paradigm after stroke: enhancing fiber growth and training of the brain at the right moment. *Front Hum Neurosci* 2014; 7: 911.
- Davila D and Torres-Aleman I. Neuronal death by oxidative stress involves activation of FOXO3 through a Two-Arm pathway that activates stress kinases and attenuates insulin-like growth factor I signaling. *Mol Biol Cell* 2008; 19: 2014–2025.
- Fernandez AM, Fernandez S, Carrero P, et al. Calcineurin in reactive astrocytes plays a key role in the interplay between proinflammatory and anti-inflammatory signals. *J Neurosci* 2007; 27: 8745–8756.
- Doyle KP, Simon RP and Stenzel-Poore MP. Mechanisms of ischemic brain damage. *Neuropharmacology* 2008; 55: 310–318.
- Arpa J, Sanz-Gallego I, Medina-Baez J, et al. Subcutaneous insulin-like growth factor-1 treatment in spinocerebellar ataxias: an open label clinical trial. *Mov Disord* 2011; 26: 358–359.
- Hatton J, Kryscio R, Ryan M, et al. Systemic metabolic effects of combined insulin-like growth factor-I and growth hormone therapy in patients who have sustained acute traumatic brain injury. *J Neurosurg* 2006; 105: 843–852.
- Khwaja OS, Ho E, Barnes KV, et al. Safety, pharmacokinetics, and preliminary assessment of efficacy of mecasermin (recombinant human IGF-1) for the treatment of rett syndrome. *Proc Natl Acad Sci U S A* 2014; 111: 4596–4601.
- Kolevzon A, Bush L, Wang A, et al. A pilot controlled trial of insulin-like growth factor-1 in children with Phelan-McDermid syndrome. *Mol Autism* 2014; 5: 54.
- Aberg D, Jood K, Blomstrand C, et al. Serum IGF-I levels correlate to improvement of functional outcome after ischemic stroke. *J Clin Endocrinol Metab* 2011; 96: E1055–E1064.
- De Smedt A, Brouns R, Uyttenboogaart M, et al. Insulin-like growth factor I serum levels influence ischemic stroke outcome. *Stroke* 2011; 42: 2180–2185.
- Bake S, Selvamani A, Cherry J, et al. Blood brain barrier and neuroinflammation are critical targets of IGF-1-mediated neuroprotection in stroke for middle-aged female rats. *PLoS One* 2014; 9: e91427.
- Guan J, Bennet L, Gluckman PD, et al. Insulin-like growth factor-1 and post-ischemic brain injury. *Prog Neurobiol* 2003; 70: 443–462.
- Liu Y, Wang X, Li W, et al. A sensitized IGF1 treatment restores corticospinal axon-dependent functions. *Neuron* 2017; 95: 817–833 e4.
- De Geyter D, De Smedt A, Stoop W, et al. Central IGF-I receptors in the brain are instrumental to neuroprotection by systemically injected IGF-I in a rat model for ischemic stroke. *CNS Neurosci Ther* 2016; 22: 611–616.
- Liu W, D'Ercole JA and Ye P. Blunting type 1 insulin-like growth factor receptor expression exacerbates neuronal apoptosis following hypoxic/ischemic injury. *BMC Neurosci* 2011; 12: 64.
- Endres M, Piriz J, Gertz K, et al. Serum insulin-like growth factor I and ischemic brain injury. *Brain Res* 2007; 1185: 328–335.
- Yan H, Mitschelen M, Toth P, et al. Endothelin-1-induced focal cerebral ischemia in the growth hormone/IGF-1 deficient lewis dwarf rat. *J Gerontol A Biol Sci Med Sci* 2014; 69: 1353–1362.
- De Magalhaes Filho CD, Kappeler L, Dupont J, et al. Deleting IGF-1 receptor from forebrain neurons confers neuroprotection during stroke and upregulates endocrine somatotropin. *J Cereb Blood Flow Metab* 2016; 37: 396–412.
- Ganat YM, Silbereis J, Cave C, et al. Early postnatal astroglial cells produce multilineage precursors

- and neural stem cells in vivo. *J Neurosci* 2006; 26: 8609–8621.
25. Garcia-Caceres C, Quarta C, Varela L, et al. Astrocytic insulin signaling couples brain glucose uptake with nutrient availability. *Cell* 2016; 166: 867–880.
  26. Hankey GJ. Ischemic events after intracerebral hemorrhage: a new target for secondary prevention. *JAMA Neurol* 2021; 78: 795–797.
  27. Pozo-Rodríguez A, Gradillas A, Serrano J, et al. New synthesis and promising neuroprotective role in experimental ischemic stroke of ONO-1714. *Eur J Med Chem* 2012; 54: 439–446.
  28. Bouet V, Boulouard M, Toutain J, et al. The adhesive removal test: a sensitive method to assess sensorimotor deficits in mice. *Nat Protoc* 2009; 4: 1560–1564.
  29. Li Y, Chopp M, Chen J, et al. Intraatrial transplantation of bone marrow nonhematopoietic cells improves functional recovery after stroke in adult mice. *J Cereb Blood Flow Metab* 2000; 20: 1311–1319.
  30. Trejo JL, Carro E and Torres-Aleman I. Circulating insulin-like growth factor I mediates exercise-induced increases in the number of new neurons in the adult hippocampus. *J Neurosci* 2001; 21: 1628–1634.
  31. Pfaffl MW. A new mathematical model for relative quantification in real-time RT-PCR. *Nucleic Acids Res* 2001; 29: e45.
  32. Shen XY, Gao ZK, Han Y, et al. Activation and role of astrocytes in ischemic stroke. *Front Cell Neurosci* 2021; 15: 755955.
  33. Okoreeh AK, Bake S and Sohrabji F. Astrocyte-specific insulin-like growth factor-1 gene transfer in aging female rats improves stroke outcomes. *Glia* 2017; 65: 1043–1058.
  34. Wiese S, Karus M and Faissner A. Astrocytes as a source for extracellular matrix molecules and cytokines. *Front Pharmacol* 2012; 3: 120.
  35. Lambertsen KL, Clausen BH, Babcock AA, et al. Microglia protect neurons against ischemia by synthesis of tumor necrosis factor. *J Neurosci* 2009; 29: 1319–1330.
  36. Offner H, Subramanian S, Parker SM, et al. Experimental stroke induces massive, rapid activation of the peripheral immune system. *J Cereb Blood Flow Metab* 2005; 26: 654–665.
  37. Owens T, Babcock AA, Millward JM, et al. Cytokine and chemokine inter-regulation in the inflamed or injured CNS. *Brain Res Brain Res Rev* 2005; 48: 178–184.
  38. Ding S. Dynamic reactive astrocytes after focal ischemia. *Neural Regen Res* 2014; 9: 2048–2052.
  39. Takeda H, Yamaguchi T, Yano H, et al. Microglial metabolic disturbances and neuroinflammation in cerebral infarction. *J Pharmacol Sci* 2021; 145: 130–139.
  40. Badaut J, Ashwal S and Obenaus A. Aquaporins in cerebrovascular disease: a target for treatment of brain edema? *Cerebrovasc Dis* 2011; 31: 521–531.
  41. Kitchen P, Salman MM, Halsey AM, et al. Targeting aquaporin-4 subcellular localization to treat Central nervous system edema. *Cell* 2020; 181: 784–799 e19.
  42. Escartin C and Bonvento G. Targeted activation of astrocytes: a potential neuroprotective strategy. *Mol Neurobiol* 2008; 38: 231–241.
  43. Freude S, Schilbach K, Hettich MM, et al. Neuron-specific deletion of a single copy of the insulin-like growth factor-1 receptor gene reduces fat accumulation during aging. *Horm Metab Res* 2012; 44: 99–104.
  44. Biondi O, Branchu J, Ben Salah A, et al. IGF-1R reduction triggers neuroprotective signaling pathways in spinal muscular atrophy mice. *J Neurosci* 2015; 35: 12063–12079.
  45. Gontier G, George C, Chaker Z, et al. Blocking IGF signaling in adult neurons alleviates Alzheimer's disease pathology through amyloid-beta clearance. *J Neurosci* 2015; 35: 11500–11513.
  46. Cohen E, Paulsson JF, Blinder P, et al. Reduced IGF-1 signaling delays age-associated proteotoxicity in mice. *Cell* 2009; 139: 1157–1169.
  47. Garcia-Segura LM, Rodriguez JR and Torres-Aleman I. Localization of the insulin-like growth factor I receptor in the cerebellum and hypothalamus of adult rats: an electron microscopic study. *J Neurocytol* 1997; 26: 479–490.
  48. Gazit N, Vertkin I, Shapira I, et al. IGF-1 receptor differentially regulates spontaneous and evoked transmission via mitochondria at hippocampal synapses. *Neuron* 2016; 89: 583–597. (doi:10.1016/j.neuron.2015.12.034): 1–15.
  49. Mardinly AR, Spiegel I, Patrizi A, et al. Sensory experience regulates cortical inhibition by inducing IGF1 in VIP neurons. *Nature* 2016; 531: 371–375.
  50. Hayes CA, Morgan NI, Thomas KC, et al. Neuronal and astrocyte insulin-like growth factor-1 signaling differentially modulates ischemic stroke damage. *bioRxiv* 2023. DOI: 10.1101/2023.04.02.535245.
  51. Bake S, Okoreeh AK, Alaniz RC, et al. Insulin-Like growth factor (IGF)-1 modulates endothelial blood brain barrier function in ischemic middle-aged female rats. *Endocrinology* 2015; 157: en20151840–69.
  52. Lee WH, Clemens JA and Bondy CA. Insulin-like growth factors in the response to cerebral ischemia. *Mol Cell Neurosci* 1992; 3: 36–43.
  53. Hernandez VG, Lechtenberg KJ, Peterson TC, et al. Transcriptome analysis reveals microglia and astrocytes to be distinct regulators of inflammation in the hyperacute and acute phases after stroke. *Glia* 2023; 71: 1960–1984.
  54. Liang Q, Su L, Zhang D, et al. CD93 negatively regulates astrogenesis in response to MMRN2 through the transcriptional repressor ZFP503 in the developing brain. *Proc Natl Acad Sci U S A* 2020; 117: 9413–9422.
  55. Kalinowska A and Losy J. PECAM-1, a key player in neuroinflammation. *Eur J Neurol* 2006; 13: 1284–1290.
  56. Tucić M, Stamenković V and Andjus P. The extracellular matrix glycoprotein tenascin C and adult neurogenesis. *Front Cell Dev Biol* 2021; 9: 674199.
  57. Chavez JC and LaManna JC. Activation of hypoxia-inducible factor-1 in the rat cerebral cortex after transient global ischemia: potential role of insulin-like growth factor-1. *J Neurosci* 2002; 22: 8922–8931.
  58. Ryu WS, Chung J, Schellingerhout D, et al. Biological mechanism of sex difference in stroke manifestation and outcomes. *Neurology* 2023; 100: e2490–e2503.

59. Bushnell CD, Chaturvedi S, Gage KR, et al. Sex differences in stroke: challenges and opportunities. *J Cereb Blood Flow Metab* 2018; 38: 2179–2191.
60. Jia C, Lovins C, Malone HM, et al. Female-specific neuroprotection after ischemic stroke by vitronectin-focal adhesion kinase inhibition. *J Cereb Blood Flow Metab* 2022; 42: 1961–1974.
61. Pekny M and Pekna M. Astrocyte reactivity and reactive astrogliosis: costs and benefits. *Physiol Rev* 2014; 94: 1077–1098.
62. Witcher KG, Eiferman DS and Godbout JP. Priming the inflammatory pump of the CNS after traumatic brain injury. *Trends Neurosci* 2015; 38: 609–620.
63. Morizawa YM, Hirayama Y, Ohno N, et al. Reactive astrocytes function as phagocytes after brain ischemia via ABCA1-mediated pathway. *Nat Commun* 2017; 8: 28.
64. Jiwaji Z, Tiwari SS, Avilés-Reyes RX, et al. Reactive astrocytes acquire neuroprotective as well as deleterious signatures in response to tau and A $\beta$  pathology. *Nat Commun* 2022; 13: 135.
65. Koizumi S, Hirayama Y and Morizawa YM. New roles of reactive astrocytes in the brain; an organizer of cerebral ischemia. *Neurochem Int* 2018; 119: 107–114.
66. Cherry JD, Meng G, Daley S, et al. CCL2 is associated with microglia and macrophage recruitment in chronic traumatic encephalopathy. *J Neuroinflammation* 2020; 17: 370.
67. Liddel SA, Guttenplan KA, Clarke LE, et al. Neurotoxic reactive astrocytes are induced by activated microglia. *Nature* 2017; 541: 481–487.
68. Abe N, Nishihara T, Yorozuya T, et al. Microglia and macrophages in the pathological central and peripheral nervous systems. *Cells* 2020; 9: 2132.
69. Lou N, Takano T, Pei Y, et al. Purinergic receptor P2RY12-dependent microglial closure of the injured blood-brain barrier. *Proc Natl Acad Sci U S A* 2016; 113: 1074–1079.
70. Beck H, Semisch M, Culmsee C, et al. Egr-1 regulates expression of the glial scar component phosphacan in astrocytes after experimental stroke. *Am J Pathol* 2008; 173: 77–92.
71. Tureyen K, Brooks N, Bowen K, et al. Transcription factor early growth response-1 induction mediates inflammatory gene expression and brain damage following transient focal ischemia. *J Neurochem* 2008; 105: 1313–1324.
72. Ribeiro M. d C, Hirt L, Bogousslavsky J, et al. Time course of aquaporin expression after transient focal cerebral ischemia in mice. *J Neurosci Res* 2006; 83: 1231–1240.
73. Takano T, Tian G-F, Peng W, et al. Astrocyte-mediated control of cerebral blood flow. *Nat Neurosci* 2006; 9: 260–267.
74. Pinard E, Nallet H, MacKenzie ET, et al. Penumbra microcirculatory changes associated with peri-infarct depolarizations in the rat. *Stroke* 2002; 33: 606–612.
75. Ngai AC and Winn HR. Modulation of cerebral arteriolar diameter by intraluminal flow and pressure. *Circ Res* 1995; 77: 832–840.
76. Fernandez AM, Martinez-Rachadell L, Navarrete M, et al. Insulin regulates neurovascular coupling through astrocytes. *Proc Natl Acad Sci U S A* 2022; 119: e2204527119.
77. Liu L, Zhang K, Sandoval H, et al. Glial lipid droplets and ROS induced by mitochondrial defects promote neurodegeneration. *Cell* 2015; 160: 177–190.
78. Choudhury GR and Ding S. Reactive astrocytes and therapeutic potential in focal ischemic stroke. *Neurobiol Dis* 2016; 85: 234–244.
79. Munive V, Santi A and Torres-Aleman I. A concerted action of estradiol and insulin like growth factor I underlies sex differences in mood regulation by exercise. *Sci Rep* 2016; 6: 25969–269.
80. Howard VJ and McDonnell MN. Physical activity in primary stroke prevention: just do it!. *Stroke* 2015; 46: 1735–1739.